Sailing with solar and planetary radiation pressure

Sailing with Solar and Planetary Radiation Pressure

Alessia De Iuliis[a,*], Francesco Ciampa[b], Leonard Felicetti[c], Matteo Ceriotti[d]

[a] *Department of Aerospace Engineering, Politecnico di Torino, Corso Duca degli Abruzzi,24, 10129, Turin, Italy*
[b] *Department of Mechanical Engineering Sciences, University of Surrey, Stag Hill, Guildford GU2 7XH, Surrey, UK*
[c] *School of Aerospace, Transport and Manufacturing, Cranfield University, College Rd, Bedford MK43 0AL, Cranfield, UK*
[d] *James Watt School of Engineering, University of Glasgow, G12 8QQ, Glasgow, UK*

Abstract

Literature on solar sailing has thus far mostly considered solar radiation pressure (SRP) as the only contribution to sail force. However, considering a sail in a planetary mission scenario, a new contribution can be added. Since the planet itself emits radiation, this generates a radial planetary radiation pressure (PRP) that is also exerted on the sail. Hence, this work studies the combined effects of both SRP and PRP on a sail for two case studies, i.e. Earth and Venus. In proximity of the Earth, the effect of PRP can be significant under specific conditions. Around Venus, instead, PRP is by far the dominating contribution. These combined effects have been studied for single- and double-sided reflective coating and including eclipse. Results show potential increase in the net acceleration and a change in the optimal attitude to maximise the acceleration in a given direction. Moreover, an increasing semi-major axis manoeuvre is shown with and without PRP, to quantify the difference on a real-case scenario.

Keywords: Planetary sail, solar radiation pressure, planetary radiation pressure, albedo, black-body radiation

*Corresponding author, alessia.deiuliis@studenti.polito.it

Nomenclature

A	sail surface, m^2
a	semi-major axis of sail orbit, m
$\tilde{a}$	absorption coefficient
$\mathbf{a}$	sail acceleration, ms^{-2}
a_0	sail characteristic acceleration, ms^{-2}
$a_{0,s}$	specific sail characteristic acceleration, ms^{-2}
c	light speed, ms^{-1}
F	view factor
$\mathbf{h}$	orbital out of plane unit vector
L_P	planet luminosity, W
m	sail mass, kg
$\hat{\mathbf{n}}$, $\hat{\mathbf{t}}$	unit vector normal and transverse to the sail surface
$\mathbf{n}^*$	unit vector normal to the orbital velocity
P	local pressure on sail surface, Nm^{-2}
q_a	albedo flux, Wm^{-2}
R_P	planet radius, m
R_{S-P}	Sun-planet distance, m
r	distance between the sail and the origin, m
$\tilde{r}$	reflection coefficient
$\hat{\mathbf{r}}$	radial direction
T_P	planet temperature, K
$\hat{\mathbf{u}}_i$	direction of the solar radiation
$\mathbf{v}$	unit vector along the orbital velocity
α	pitch angle, deg
δ	angle between $\hat{\mathbf{n}}$ and $\hat{\mathbf{r}}$, deg

σ	attitude angle, deg
σ^*	sail loading, kgm^{-2}
$\overline{\sigma}$	Stefan-Boltzmann constant, $Wm^{-2}K^{-4}$
β	reflection angle, rad
ζ	fraction of the total solar radiation reflected back into space
ARP	Albedo radiation pressure
BBRP	Black-body radiation pressure

Subscripts

0	Initial
PRP	Planetary radiation pressure
SRP	Solar radiation pressure
i	Incident
a	Absorbed
r	Reflected

1. Introduction

Solar sailing is the unique form of propulsion that transcends reliance on reaction mass. A solar sail gains momentum from an ambient source, the photon radiation pressure. Hence, it is possible to gain or reduce the orbital angular momentum controlling the orientation of the sail. The orbital dynamics of solar sails uses a small continuous thrust to modify the orbit over an extended period of time. This concept is similar to the low-thrust electric propulsion system dynamics; thanks to this, solar sails can be used in a wide range of missions such as lunar fly-bys (Eguchi et al., 1993), (Fekete, 1992), inner (Garner et al., 2001) and outer (Leipold, 2000) solar system rendezvous missions, and could offer potentially low-cost operations (Frisbee and Brophy, 1997) and flexible manoeuvres for exploring the solar system (Colasurdo and Casalino, 2001) and planetary orbits.

In the work of Macdonald and McInnes (Macdonald and McInnes, 2011), some potential solar sails applications are presented. Two highly significant planet-centred solar sail concepts are the GeoSail (Macdonald et al. (2007), Mengali et al. (2007), Lappas et al. (2009)) and the Mercury Sun-Synchronous Orbiter (Leipold et al., 1996). Both use a solar sail to independently vary a single orbit parameter. Another application of solar sailing in planet-centred trajectory is the use of the sail to perform an escape manoeuvre. Coverstone

and Prussing (2003) developed a technique for escaping the Earth using a solar sail with a spacecraft initially in a geosynchronous transfer orbit (GTO). A more accurate study on Earth escape strategies has been conducted by Macdonald and McInnes (2005), using blending locally optimal control laws. These blended sail-control algorithms, explicitly independent of time, provide near-optimal escape trajectories maintaining a safe minimum altitude. When the sail is in atmosphere, aerodynamic forces are exerted on the sail too: Stolbunov et al. (2013) developed a dynamic model of the sail in three-dimension (3D) and the expressions for the acceleration due to both solar radiation pressure (SRP) and aerodynamic forces. Mengali and Quarta (2005) also analysed the effect of aerodynamic drag on solar sail trajectories, to obtain near-minimum time manoeuvres for low characteristic acceleration. In this work the sail is treated as a flat plate and a hyperthermal flow model is assumed.

All these studies on planetary solar sailing do not consider that the planet is a body that emits radiations and reflects part of the radiations coming from the Sun. The planet, being a body in thermodynamic equilibrium with its environment, emits the so-called black-body radiation. This radiation is emitted uniformly in all directions, with most of the energy emitted in the infrared range. The specific spectrum and intensity of this radiation depends only on the body temperature (Larson and Wertz, 1992). Moreover, the radiation coming from the Sun is reflected diffusely from the planet surface into the outer space as a function of the position of the Sun. This radiation is known as albedo and it varies with geological and environmental features (Lyle et al., 1971). The sum of the black-body radiation pressure (BBRP) and the albedo radiation pressure (ARP) will be called planetary radiation pressure (PRP). These photons will also hit the sail film, effecting the sail acceleration and thus changing its dynamics. The contribution of the ARP has been studied in the literature by Grøtte and Holzinger (2017). The authors have studied the combined effects of SRP and ARP in the circular restricted three body problem, for a system consisting of the Sun, a reflective minor body, and the solar sail. The results show the presence of additional artificial equilibrium points in the volume between L_1 and L_2 points.

The contribution of the PRP has never been fully considered for planetary sails. Hence in this work we aim to explore the combined effects of both solar radiation pressure (SRP) and planetary radiation pressure (PRP) on a sail orbiting around a planet (e.g. Earth or Venus), and quantify its effects on an orbit with respect to the traditional case of SRP-only. We studied these combined effects around a planet for two types of sail: single- and double-sided reflective coating. The optimal attitude that maximises the acceleration along the radial direction, considering SRP and PRP, is identified. Results show potential increase in the net acceleration and a change in optimal attitude to maximise the radial propulsive acceleration. To quantify these effects on practical real-case scenario, an optimal semi-major axis increase trajectory is shown with and without the PRP.

In Sec. 2, SRP and PRP accelerations models are presented together with the simulation scenarios. The study proceeds in Sec. 3 with the maximisation

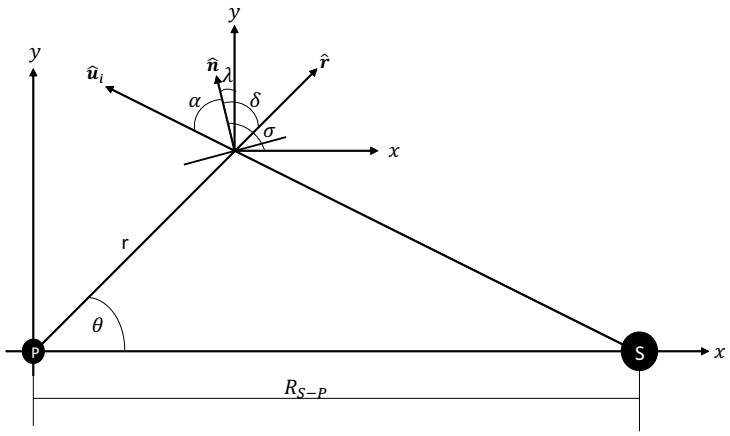

Figure 1: Reference frame for a sail orbiting around a planet.

of the radial propulsive acceleration for different planets considering different contributions (solar, black-body, and albedo). In Sec. 4, propelled trajectories for increasing the orbital energy of a sail around a planet are shown. Finally, conclusions are presented in Sec. 5.

2. Models

A two dimensional two-body model is used to simplify the problem, and the sail is considered to belong to the ecliptic plane. The reference frame is centred in the planet, as can be seen in Fig. 1.

The Sun, which is assumed to be an inertial reference system, lies along the x-axis at a distance of R_{S-P} from the origin. The y-axis is normal to x in the ecliptic plane. The distance between the sail and the origin is $r = \sqrt{x^2 + y^2}$ and the angle between r and x-axis is θ. The sail used for the study has a flat geometry. It is possible to define the unit vector normal to the sail normal surface $\hat{\mathbf{n}}$:

$$\hat{\mathbf{n}} = [\cos\sigma, \sin\sigma] \tag{1}$$

and $\hat{\mathbf{t}}$ as the transverse unit vector normal to $\hat{\mathbf{n}}$ with components

$$\hat{\mathbf{t}} = [-\sin\sigma, \cos\sigma] \tag{2}$$

where σ expresses the attitude of the sail, which is defined as the angle between $\hat{\mathbf{n}}$ and the positive x-axis and is measured counter-clockwise between 0 and 2π. The second angle used for the attitude is λ, measured from $\hat{\mathbf{n}}$ to the y-axis. The latter is used in the case of a double-reflective coated sail and, due to the symmetry of the problem, it lies between 0 and π.

In order to define the solar sail performance, a standard metric is introduced. The solar sail characteristic acceleration is defined as the SRP acceleration experienced by a solar sail facing the Sun at a distance of one astronomical unit, that is

$$a_0 = (2\tilde{r} + \tilde{a})\frac{P_{SRP}}{\sigma^*} \tag{3}$$

where P_{SRP} is the photon pressure and $\sigma^* = \frac{m}{A}$ is the sail loading, expressed as the sail mass per unit area (A is the sail area, m is its mass). The star is used to avoid confusion with the attitude angle σ. The reflection ($\tilde{r}$) and absorption ($\tilde{a}$) coefficients are introduced to consider the optical characteristics of the sail. The factor 2 added in Eq. (3) considers that the photons that hit the sail film are reflected, doubling the pressure exerted on the sail. In this work, emission by re-radiation is not considered since it is assumed that incident photons are re-emitted by reflection only (McInnes, 1999). This leads to a constrain that may be written as

$$\tilde{a} = 1 - \tilde{r} \tag{4}$$

The absorption coefficient $\tilde{a}$ takes into account the fact that a portion of the photons impacting the sail film is absorbed and the remaining part is reflected.

Since the study is conducted for different planets, a specific characteristic acceleration ($a_{0,s}$) is defined as the acceleration experienced by a sail facing the Sun at a distance equal to the mean distance between the planet and the Sun, with the value of the pressure at the heliocentric distance of the planet.

This study considers the combined effects of both SRP and PRP. With reference to Fig. 1, the photons emitted by the Sun generate a force exerted along the unit vector $\hat{\mathbf{u}}_i$, instead the unit vector $\hat{\mathbf{r}}$ shows the direction of the planetary radiation, radial from the planet. The angle between $\hat{\mathbf{n}}$ and $\hat{\mathbf{u}}_i$ is the sail pitch angle (α) and the angle between the direction of the planetary radiation pressure ($\hat{\mathbf{r}}$) and the solar sail normal unit vector ($\hat{\mathbf{n}}$) is δ. These two angles range in the interval $[0, \pi]$ to consider the radiation exerted on both the front and on the back of the sail.

We considered eclipses, modelled using a cylindrical eclipse model. In this case the Sun is assumed to be infinitely far away from the planet so that the divergence of the rays is small and the light rays can be considered as parallel, without making a consistent difference. This produces a cylindrical planet shadow with a radius equal to the planet radius. In eclipse, the only pressure exerted on the sail is the PRP.

2.1. Effect of the Solar Radiation Pressure

In this subsection the model used to express the sail acceleration due to the SRP is shown. Considering the definition of $\hat{\mathbf{n}}$ and $\hat{\mathbf{t}}$ given in Eqs. (1) and (2), it is possible to express $\hat{\mathbf{u}}_\mathbf{i}$ as:

$$\hat{\mathbf{u}}_i = \cos\alpha\ \hat{\mathbf{n}} + \sin\alpha\ \hat{\mathbf{t}} \tag{5}$$

The acceleration exerted on the sail due to absorption can be found considering that α is the angle between the incoming radiation and the normal vector:

$$\mathbf{a}_{a,SRP} = \tilde{a}\frac{P_{SRP}}{\sigma^*}\cos\alpha\ \hat{\mathbf{u}}_\mathbf{i} \tag{6}$$

where P_{SRP} is the radiation pressure. Resolving this force in normal and transverse components, using Eq. (5)

$$\mathbf{a}_{a,SRP} = \tilde{a}\frac{P_{SRP}}{\sigma^*}\left(\cos^2\alpha\ \hat{\mathbf{n}} + \cos\alpha\sin\alpha\ \hat{\mathbf{t}}\right) \tag{7}$$

As with regards to the reflected photons, they generate an acceleration equal to:

$$\mathbf{a}_{r,SRP} = 2\tilde{r}\frac{P_{SRP}}{\sigma^*}\cos^2\alpha\ \hat{\mathbf{n}} \tag{8}$$

Hence, the acceleration due to the solar radiation pressure, on a sail with optical characteristics can be written as the sum of the acceleration along $\hat{\mathbf{n}}$ due to the absorbed and reflected photons and the acceleration along $\hat{\mathbf{t}}$ generated by the absorbed photons:

$$\mathbf{a}_{SRP} = \mathbf{a}_{a,SRP} + \mathbf{a}_{r,SRP} \tag{9}$$

2.2. Effect of the Planetary Radiation Pressure

When the sail is orbiting in the vicinity of a planet, radiation coming from the planet itself exerted on the sail, should be considered. For this reason, in this section, the model used to describe the PRP force is shown and the description of the two different types of radiation (BBRP and ARP) will follow.

In the case of SRP, the source was considered as a point infinitely far from the sail. However, this approximation might not be suitable for a close-by planet, hence the celestial body is modelled as a disc with uniform brightness. This means that it will appear equally bright when viewed from any aspect angle. The variation of the direction of incidence radiation from different parts of the planet will be included.

To better explain the effect of radiation pressure on a solar sail, we consider radiative transfer. The derivation by McInnes (1999) is adopted to find the expression for a PRP acceleration with the planet modelled as a disc, considering (in first approximation) a radially-oriented solar sail from a uniformly bright, finite angular size disc:

$$P_{PRP}(r) = \frac{L_P}{3\pi c R_P^2}\left(1 - \left(1 - \left(\frac{R_P}{r}\right)^2\right)^{3/2}\right) \tag{10}$$

Where L_P is the planetary luminosity, which is defined as

$$L_P = L_{P,BBRP} + L_{P,ARP} \tag{11}$$

The acceleration can be modelled with an optical model, with an absorption coefficient $\tilde{a}$ and a reflection coefficient $\tilde{r}$ (considered to be the same for both SRP and PRP). Hence it can be resolved in normal and transverse component:

$$\begin{aligned}\mathbf{a}_{a,PRP} =&\tilde{a}\frac{L_P}{3\pi c\sigma^* R_P^2}\left(1-\left(1-\left(\frac{R_P}{r}\right)^2\right)^{3/2}\right)\\ &\left(\cos^2\delta\ \hat{\mathbf{n}}+\cos\delta\sin\delta\ \hat{\mathbf{t}}\right)\end{aligned} \tag{12}$$

$$\mathbf{a}_{r,PRP} = \tilde{r}\frac{L_P}{3\pi c\sigma^* R_P^2}\left(1-\left(1-\left(\frac{R_P}{r}\right)^2\right)^{3/2}\right)\left(\cos^2\delta\ \hat{\mathbf{n}}\right) \tag{13}$$

As mentioned, the radiation due by to planet is of two different origins: the first one is the black-body radiation (emitted by the planet), and the second one is the albedo (reflected from the Sun). In the following subsections, the models used to describe these phenomena will be discussed.

2.2.1. Black Body Radiation Pressure

In this study, the planet is considered as a black body in equilibrium with its environment, emitting the so-called black body radiation (ideal and diffuse emitter). The energy is radiated isotropically and most of it will be in the infrared range (Larson and Wertz, 1992). Moreover, the specific spectrum and intensity only depends on the body's temperature. Therefore the planet will emit according to the Stefan-Boltzmann law (Stefan, 1879), with luminosity:

$$L_{P,BBRP} = 4\pi R_P^2 \overline{\sigma} T_P^4 \tag{14}$$

where R_P is the radius of the planet, T_P is its mean temperature and $\overline{\sigma} = 5.670370\cdot 10^{-8}$ W/(m^2 K^4) is the Stefan-Boltzmann constant. Substituting this luminosity in Eqs. (12) and (13) we have the expression for the acceleration due to the BBRP ($\mathbf{a}_{BBRP}$).

2.2.2. Albedo Radiation Pressure

The Sun emits its radiation equally in all directions and a part of it strikes the planet. Of all this amount, the planet reflects a fraction of this flux and this is known as albedo. It varies with both geological and environmental features of the planet.

The calculation of the power generated due to albedo is based on Ref. (Thornton, 1996). First of all, the fraction of the total radiant energy leaving the planet that arrives at the surface of the solar sail is considered by a view factor F.

Moreover, ζ is the fraction of the total solar radiation striking the Earth that is reflected back into space. It varies both geographically and seasonally, however using $\zeta = 0.36$ gives good approximation (Thornton, 1996). Albedo

occurs over the day side of the planet only, and it varies as the cosine of the reflection angle β. It is now possible to calculate the albedo flux as:

$$q_a = W_P \zeta F \cos\beta \tag{15}$$

where W_P is the solar flux at planet orbit. To calculate the power used in Eqs. (12) and (13), this flux should be multiplied by the disc surface, that is the area struck by the solar radiation that reflects the radiation back into space. This is a circle of the radius of the planet.

It is now possible to express the luminosity due to the albedo as:

$$L_{P,ARP} = q_a \ \pi R_P^2 \tag{16}$$

The two contributions expressed in Eqs. (14) and (16) can then be used in Eqs. (12) and (13) and they will express the accelerations due to BBRP and ARP, respectively, and the sum of them is the contribution due to the PRP. The total acceleration experienced by the sail, when it is out of the eclipse region can be written as:

$$\mathbf{a} = \mathbf{a}_{a,SRP} + \mathbf{a}_{r,SRP} + \mathbf{a}_{a,PRP} + \mathbf{a}_{r,PRP} \tag{17}$$

When the sail is in eclipse, for $x < 0$ and $y \subset [-R_P, R_P]$, the terms due to the SRP are set equal to zero, and the sail is subject to the BBRP only, since the albedo occurs only in daylight.

2.3. Simulation Scenarios

In this work, a sail with a sail loading $\sigma^* = 0.1$ kg/m^2 is considered. The ratio of the resulting acceleration to the specific characteristic acceleration ($a_{0,s}$) of the planet is considered as the main performance parameter. Hence, results do not depend on the sail lightness number and they are valid for every flat sail regardless of its mass or area.

The analysis has been conducted for Earth and Venus. For each planet the specific characteristic acceleration $a_{0,s}$ is calculated using Eq. (3). Core values for each scenario are presented in Table 1.

To add the contribution of the BBRP, the luminosity should be calculated according to the Stefan-Boltzmann law (Eq. (14)). Values of planetary radius (R_P), mean temperature of the planet ($T_{m,P}$) and the corresponding luminosity (L_{BBRP}) are shown in Table 1. As for the pressure due to albedo, it is not possible to calculate a general value since it changes both with the point and the attitude of the sail (Eq. (15)). The value of the solar flux in planet orbit (W) is also reported in the Table 1 and it is used in the calculation of the luminosity.

The study is conducted for two kinds of sail with different optical properties for the front and back side of the sail film. The first is a single-sided reflective coating sail in which the reflective front side has a reflection coefficient $\tilde{r}_f = 0.9$, whereas the back side has $\tilde{r}_b = 0$. This means that all the photons are

Table 1: Solar radiation pressure at the mean distance between the Sun and the planet, specific characteristic acceleration, planet radius, planet mean temperature, luminosity due to the BBRP and solar flux in orbit for Earth and Venus.

	Venus	Earth
P_{SRP} [N/m^2]	$8.72 \cdot 10^{-6}$	$4.56 \cdot 10^{-6}$
$a_{0,s}$ [m/s^2]	$1{,}65 \cdot 10^{-4}$	$8{,}66 \cdot 10^{-5}$
R_P [m]	$6070 \cdot 10^3$	$6378 \cdot 10^3$
$T_{m,P}$ [K]	735.15	279.00
L_{BBRP} [W]	$1.6679 \cdot 10^{18}$	$1.7562 \cdot 10^{17}$
W [W/m^2]	2604	1350

absorbed by the back side of the sail. The second sail, instead, has a double-sided reflective coating, with a reflection coefficient $\tilde{r} = 0.9$ for both sides. In this work a sail coated with Aluminium has been considered. Since Aluminium reflectivity varies of only 12% considering a wavelengths range between [300nm - 2500nm] (Bass et al., 2009), it is reasonable approximation to use the same optical properties for the three different contributions: solar, black body and albedo radiation.

3. Maximisation of sail acceleration

This section focuses on finding the attitude angle σ that enables the sail to have a maximum acceleration along a given direction by considering both SRP and PRP. Once this angle is known, it could be used in the dynamics of the sail to perform manoeuvres. Because of the complexity of finding an analytical law explicitly, a numerical approach is proposed in this paper. In order to show the methodology and to highlight the effect of the PRP in particular, this section will address the problem of maximisation of the radial component of the acceleration.

Given a point in space, and a particular desired direction for the acceleration, the analysis scans the attitude angles σ over the entire circle, using 1000 values from 0 to 2π, and the corresponding acceleration along the given direction is calculated for each angle. Among these accelerations, the one that maximises a certain objective is identified, and the corresponding angle is chosen as the optimal attitude for the sail in that point. The objective varies according to the different case-studies; for example, a maximisation or minimisation of the acceleration magnitude along a given direction may be required.

In order to show and compare the results, the approach used at a single point is subsequently applied in a grid of (500×500) points centred in the planet. Since the sail is to orbit above the atmosphere, only those points at least 400 km above the planet surface are taken into account.

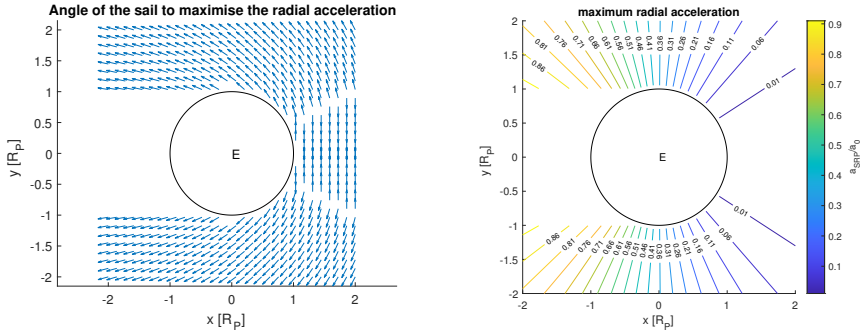

(a) Direction of the sail normal. (b) Contour of a_{SRP}/a_0.

Figure 2: Maximisation of radial acceleration, for a single-sided coating sail around Earth subject to SRP.

Results obtained following this methodology are presented in the following sections.

3.1. Maximum Radial Acceleration

In this section, results are shown considering the maximisation of the radial acceleration.

Results are presented using two families of plots: one shows the direction of the sail normal unit vector $\hat{\mathbf{n}}$ as a vector field, and the other shows the contour of the normalised sail acceleration (over the specific characteristic acceleration). First the case of SRP only is considered, then the contribution of the PRP is added and the comparison between the scenarios is performed.

3.1.1. Earth Scenario

In this scenario, the sail is considered around the Earth. The results in the case of a maximum radial acceleration, considering the presence of SRP only, are presented in Fig. 2. The direction of the sail normal that maximises the radial acceleration is shown in Fig. 2a. For $x < 0$ and $y \subset [-R_P, R_P]$ the sail is placed is the eclipse region, since the Sun is always considered fixed on the right of the planet. Here no force is exerted on the sail since the sunlight is blocked by the planet itself, for this reason it is meaningless to find a direction that maximises the radial acceleration. In the region $x \subset [R_P, 2R_P]$ and $y \subset [-R_P, R_P]$, the Sun gives a negative contribution along the radial direction, thus it is preferred to have a null acceleration than a negative one. Hence, the attitude angle σ is equal to 90 or 270 deg to guarantee a zero acceleration. Moreover, Fig. 2b shows that the greatest radial acceleration can be found for points with $x \subset [-2R_P, -R_P]$, where the Sun gives a positive contribution along the radial direction. The contours shown in Figs. 3b and 2b present the value of the ratio $a_{SRP+PRP}/a_0$ and a_{SRP}/a_0, respectively.

When the PRP is added, results change and they are presented in Fig. 3. The first considerable difference can be found in the eclipse region. If only

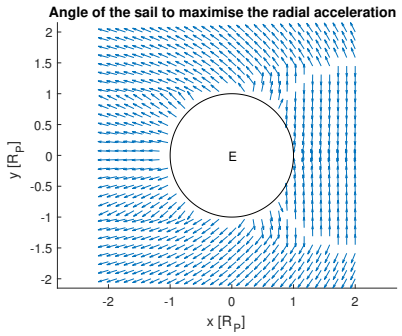

(a) Direction of the sail normal.

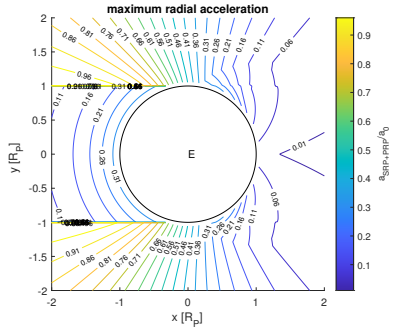

(b) Contour of $a_{SRP+PRP}/a_0$.

Figure 3: Maximisation of radial acceleration, for a single-sided coating sail around Earth subject to SRP and PRP.

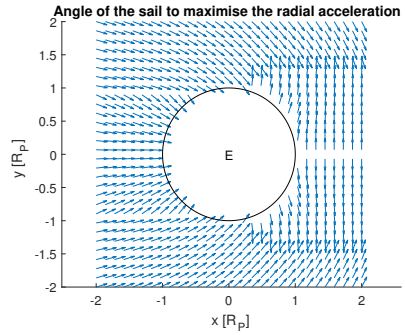

(a) Direction of the sail normal.

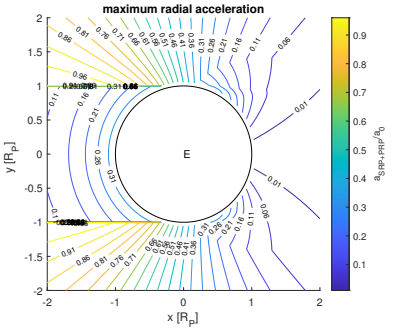

(b) Contour of $a_{SRP+PRP}/a_0$.

Figure 4: Maximisation of radial acceleration, for a double-sided coating sail around Earth subject to SRP and PRP.

Table 2: Value of the ratio of the maximum radial acceleration to the characteristic acceleration and the attitude angle σ that maximises the acceleration in the cases SRP and SRP+PRP for a single-sided reflective coated sail in the vicinity of the Earth.

Point	x km	y km	$\sigma_{max,SRP}$ rad	$\sigma_{max,SRP+PRP}$ rad	a_{SRP}/a_0	$a_{SRP+PRP}/a_0$	$a_{SRP+PRP}/a_{SRP}$
A	-1968.4	6569.7	2.6667	2.5095	0.5331	0.67063	1.2579
B	1968.4	6569.7	2.3648	1.4277	0.2143	0.3136	1.4635
C	-1968.4	-6569.7	2.6667	2.5095	0.5331	0.67063	1.2579
D	1968.4	-6569.7	2.3648	1.4277	0.2143	0.3136	1.4635

SRP is considered, the radial acceleration cannot be maximised, since no force is exerted on the sail. However, if the contribution of the PRP is taken into

account, the sail optimal attitude angle can be found, with the unit normal vector $\hat{\mathbf{n}}$ laying along the radial direction (Fig. 3a). As regards the rest of the grid, where the sail is in daylight, similar behaviour is found regardless of the introduction of the PRP. However, a difference occurs when the sail is close to the planet and for positive values of the x. In this region the sail tends to have $\hat{\mathbf{n}}$ along the radial (Fig. 3a) due to the radial radiation coming from the planet. Out of the eclipse region the trend is similar, with the highest ratio in the left part of the grid, where both SRP and PRP gives a positive contribution to the acceleration. However, in this region it is possible to calculate an increase in the radial acceleration equal to the 9% when the PRP is added. Moreover, in Fig. 3b the gap between the sunlight and eclipse area is underlined by the instantaneous change in the magnitude of the acceleration, switching from maximum to minimum values.

To summarise the results, four points around the Earth are taken into account, whose coordinates are listed in Table 2. At each of these points, the ratio of the maximum radial acceleration to the characteristic acceleration and the attitude angle σ that maximises the acceleration in the cases SRP and SRP+PRP are presented.

It is possible to state that, at every point, the addition of the PRP generates an additional contribution, enabling the sail to experience greater acceleration. Thanks to the symmetry of the problem points, A-C and B-D show the same results. The values of the optimal σ are also presented in Table 2. In the case SRP+PRP the sail changes its orientation, generating the maximum radial acceleration with lower attitude angle due to the contribution given by the planetary radiation. As regards the ratio $a_{SRP+PRP}/a_{SRP}$, Table 2 shows a maximum radial acceleration $a_{SRP+PRP}$ equals to up 1.4635 times a_{SRP}.

In Figs. 3 and 2, the considered sail had a single-sided reflective coating; if this is replaced with a double-sided reflective coating, the results change as shown in Fig. 4. The behaviour of the sail does not change considerably. Since the symmetry of the problem, the sail will be oriented specularly to the single-sided case, as can be stated comparing Figs. 3a and 4a. With regards to the radial acceleration, the trend is similar to the single-sided case: a change is present for positive x, where the region with a null acceleration gets wider. In summary, the use of a double-sided coated sail does not give substantial beneficial effects in this scenario.

3.1.2. Venus Scenario

The same analysis has been performed to analyse the effects of the radiation produced by Venus. A wider grid of points is used, with x and $y \subset [-5R_P, 5R_P]$, since the great luminosity of the planet (Table 1). Considering the presence of SRP only, Fig. 5 shows the results for the maximum radial acceleration. Fig. 5a presents the direction of the sail normal vector $\hat{\mathbf{n}}$. It is always directed towards the Sun, except for the eclipse region and for a portion with $x \subset [1R_P, 5R_P]$ and $y \subset [-2R_P, 2R_P]$ where $\sigma = 90$ or 270 deg. As already stated for the Earth, maximum radial acceleration can be found in the left part of the grid (Fig. 5b) thanks to the positive contribution of the SRP along the radial direction. Also

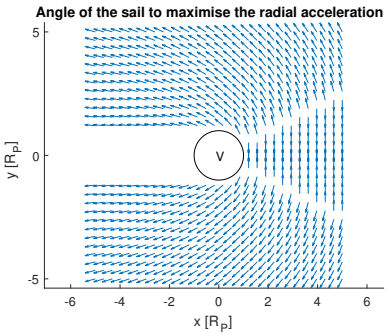

(a) Direction of the sail normal.

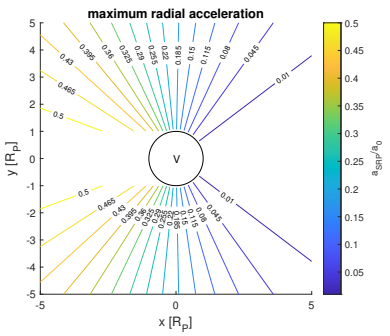

(b) Contour of a_{SRP}/a_0.

Figure 5: Maximisation of radial acceleration, for a single-sided coating sail around Venus subject to SRP.

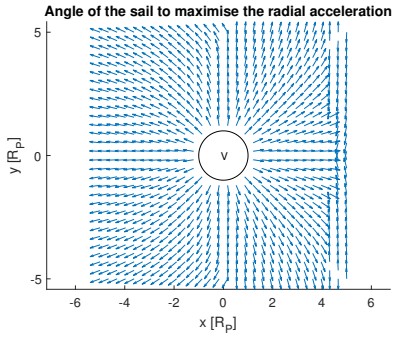

(a) Direction of the sail normal.

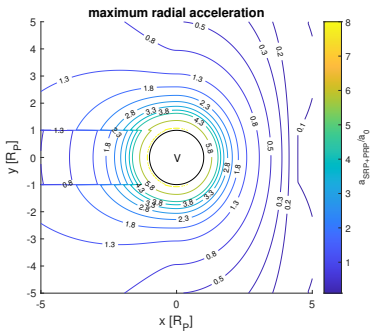

(b) Contour of $a_{SRP+PRP}/a_0$.

Figure 6: Maximisation of radial acceleration, for a single-sided coating sail around Venus subject to SRP and PRP.

in this case, a null acceleration is experienced, to avoid a negative one, when the sail is placed in points with $x \subset [1R_P, 5R_P]$ and $y \subset [-2R_P, 2R_P]$.

Table 3: Value of the ratio of the maximum radial acceleration to the characteristic acceleration and the attitude angle σ that maximises the acceleration in the cases SRP and SRP+PRP for a single-sided reflective coated sail in the vicinity of Venus.

Point	x km	y km	$\sigma_{max,SRP}$ rad	$\sigma_{max,SRP+PRP}$ rad	a_{SRP}/a_0	$a_{SRP+PRP}/a_0$	$a_{SRP+PRP}/a_{SRP}$
A	-1155.6	6751.2	2.6101	1.7548	0.2414	7.6299	31.608
B	1155.6	6751.2	2.434	1.4026	0.1434	7.5982	53.1135
C	-1155.6	-6751.2	3.673	4.5284	0.2414	7.6299	31.608
D	1155.6	-6751.2	3.8492	4.8806	0.1434	7.5982	53.1135

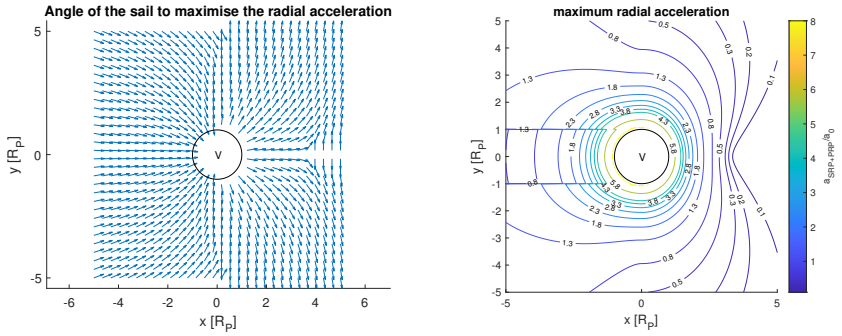

(a) Direction of the sail normal.

(b) Contour of $a_{SRP+PRP}/a_0$.

Figure 7: Maximisation of radial acceleration, for a double-sided coating sail around Venus subject to SRP and PRP.

Fig. 6 presents the results obtained when the contribution of the PRP is added. Since most contribution is given by the PRP, when the sail is close to the planet, it is just oriented along the radial direction (Fig. 6a). In this case, the eclipse region does not cause a substantial difference in the behaviour of the sail since the PRP is the main contribution everywhere. However, when the sail is placed in region with $x > 4R_P$ the behaviour of the sail returns to be similar to the case of SRP only, as can be seen in Fig. 5a. The maximum radial acceleration over the specific characteristic acceleration has the trend shown in Fig. 6b. The difference with the SRP-only case (Fig. 5b) is notable. Here, the highest value of the ratio can be found when the sail is in the region of negative x, while in Fig. 6b the closer the sail is to the planet the highest is the ratio, moving from a maximum value of ~ 0.5 (SRP) to ~ 8 when the PRP is taken into account. Moreover, the sail can now offer a non-zero acceleration even in the eclipse region.

Table 3 shows the effects of the planetary radiation for four points around Venus, to inspect the behaviour of a single-sided reflective coating sail. Specifically, it shows the value of the optimal attitude angle σ that maximises the radial acceleration and the ratio of the acceleration over the characteristic one for the two cases SRP and SRP+PRP. When the PRP is added, the sail is oriented with lower attitude angles for points A and B, while the optimal σ increases for the points C and D. This is due to the fact that the normal of the sail tends to be oriented along the radial direction to maximise the corresponding acceleration. The contribution of the PRP enables the sail to experience acceleration up to 53 times the one obtained for SRP only. Moreover, similarly to the Earth case, the symmetry of the problem leads to the same results for the points A-C and B-D.

The same analysis was conducted for a double-sided reflective coating sail: results for a maximum radial acceleration are shown in Figs. 7a and 7b. What can be underlined is the acceleration of the sail for $x \sim 5$ and $y \sim 0$. The acceleration experienced in that region for a double-sided reflective coating sail is smaller than the one for a single-sided case. This is due to the optical characteristics of the back side of the sail where the SRP is exerted and gives a negative contribution. However, also in this case, the use of a double-reflecting coating does not lead to substantial better performance of the sail.

4. Control Law for Semi-Major Axis Increase

An evaluation of the effects of the planetary radiation on the orbital motion of a sail can be performed through numerical simulation. Specifically, the aim of the study is to evaluate the additional contribution given by the PRP in an orbit raising manoeuvre. Results around Earth and Venus are shown for a single-side coating sail with a characteristic acceleration equal to 1 mm/s^2 and the cases of SRP only and SRP+PRP are analysed. To evaluate the variation of the orbital elements, Gauss' form of the Lagrange variational equations is used (Schaub and Junkins, 2018). In this case the acceleration vector $\mathbf{a}$ is written in components taken in the rotating frame $\{\mathbf{v}, \mathbf{n}^*, \mathbf{h}\}$. In this frame the direction of unit vector $\mathbf{v}$ is along the orbit velocity, $\mathbf{n}^*$ is normal to the direction of the velocity, where the dash has been added to avoid confusion with the normal direction of the sail $\hat{\mathbf{n}}$, and $\mathbf{h}$ is the out of plane component.
Gauss' variational equations in the planar case can be written as (Battin, 1999):

$$\frac{da}{dt} = \frac{2a^2 v}{\mu} a_v \tag{18}$$

$$\frac{de}{dt} = \frac{1}{v}\left(2\left(e + \cos f\right) a_v - \frac{r}{a} \sin f a_{n^*}\right) \tag{19}$$

$$\frac{d\omega}{dt} = \frac{1}{ev}\left(2 \sin f a_v + \left(2e + \frac{r}{a}\cos f\right) a_{n^*}\right) \tag{20}$$

Where:

- a is the semi-major axis;
- e is the eccentricity;
- ω is the argument of periapsis;
- f is the true anomaly;
- $\theta = \omega + f$ is the argument of latitude;
- $v = \sqrt{\mu \left(\frac{2}{r} - \frac{1}{a}\right)}$ is the sail speed.

Table 4: Initial orbital elements

Semimajor axis, a_0, km	36840
Eccentricity, e_0	0.8
Argument of periapsis, ω_0, deg	0, 90, 180, 270
True anomaly, f_0, deg	0

The MATLAB function ODE45 is used to integrate Eqs. (18), (19) and (20), with a relative and absolute tolerance equal to 1×10^{-9} and 1×10^{-10}, respectively.

The initial orbit is in the ecliptic plane with a high eccentricity, a low periapsis and four positions of the argument of the periapsis (to change the relative rotation to the Sun-line). Table 4 presents the values of the orbital elements of the starting orbit (for both the Earth and Venus scenarios) – where the periapsis is measured with respect to the x-axis, which coincides with the direction of the Sun. The trajectories with initial $\omega_0 = 0, 90, 180, 270$ deg are denominated T1, T2, T3 and T4, respectively.

To change the semi-major axis the most efficient strategy is to use a tangential control law. The variation of the semi-major axis (a) reaches maximum value at the periapsis since the velocity magnitude is the largest in that point (Gao, 2007). For this reason, it has been decided to use a control law that maximises the acceleration in the direction of the velocity (i.e. tangential) when the sail is within ± 30 deg of pericentre. This control law is sub-optimal, but since the aim of this work is to compare the results in the cases SRP and SRP+PRP, it is sufficient to use the same control law in both cases.

In the following sections, the results of the integration of the sail control law will be studied, investigating how the inclusion of the PRP affects the increase in semi-major axis.

4.1. Earth

For the Earth case, the results can be summarised in Table 5, for the four trajectories T1-T4. The Table shows the increase in semi-major axis achieved after 3 revolutions, with respect to the initial semi-major axis, when the contribution of SRP, or both SRP+PRP, are considered. Finally, the last column shows the increase offered by the SRP+PRP case over the SRP-only case.

Table 5: Semi-major axis increase considering SRP only, SRP+PRP, and gain between the former and the latter, for the Earth.

Trajectory	Increase with SRP+PRP	Increase with SRP	Gain due to PRP
T1	0.1855%	0.1547%	19.89%
T2	0.3902%	0.3858%	1.84%
T3	0.0479%	$5.71 \cdot 10^{-4}$%	8288.79%
T4	0.0131%	$1.18 \cdot 10^{-4}$%	11001.69%

To justify these results, we now present two trajectories, T2 and T3, in more detail.

Trajectory T2 considers the sail orbiting around the Earth with an initial argument of periapsis $\omega = 90\,\text{deg}$. The resulting trajectory, including a representation of the sail orientation and its normal, is presented in Fig. 8. In this and all following scenarios, the Sun is on the positive x-axis.

Figure 9 shows that the presence of the PRP gives a positive contribution to the dynamics of the sail. As highlighted in Table 5 for T2, the semi-major axis has incremented by only 1.84% more with SRP+PRP than with SRP only. Fig. 10 shows the trend of the acceleration around the periapsisis for trajectory T2. It is possible to state that the acceleration is almost always null except in the thrusting arc. However, the inclusion of the PRP does not lead to consistently greater acceleration, showing that the main role is played by the SRP in both cases.

We now consider trajectory T3, with the periapsis in the eclipse region, i.e. $\omega = 180\,\text{deg}$. Fig. 11 shows that the thrusting arc lays in the shadow region. For this reason, when only the SRP is considered, the variation of the semi-major is almost zero.

Results change adding the PRP, with a step increase of a (Fig. 12). In this case, the percentage increase between the SRP case and the SRP+PRP case is several orders of magnitude. In fact, Fig. 13 shows that the sail has an almost null acceleration throughout the orbit when the SRP is considered and a non-zero one thanks to the contribution of the PRP when the sail is in the thrusting arc. These results highlight that the PRP allows to increase the semi-major axis even if the periapsis is in eclipse.

The same study has been conducted for T1 ($\omega_0 = 0$) and T4 ($270\,\text{deg}$). Table 5 summarises the results for all four trajectories. The increase in semi-

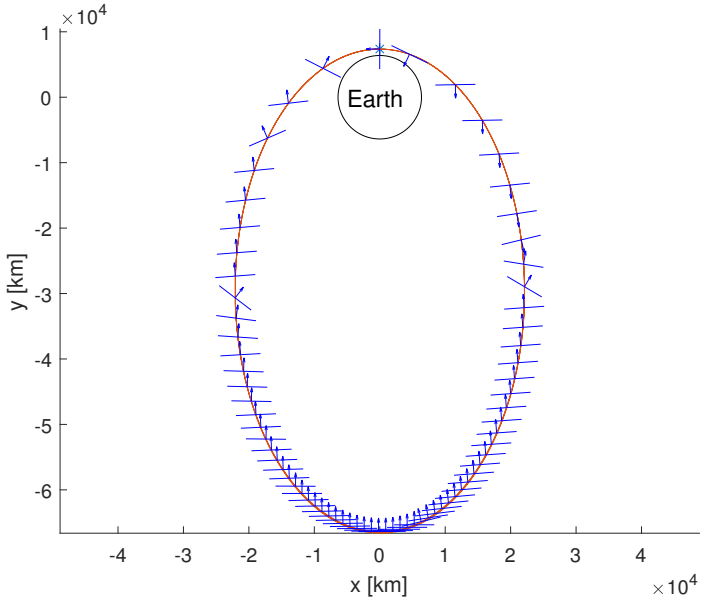

Figure 8: Trajectory around the Earth with orientation of the sail on T2 ($\omega_0 = 90\,\text{deg}$) considering SRP+PRP.

major axis is less than 1% in the best scenario (T2 considering SRP+PRP): this may not seem considerable, but it should be noted that this percentage is almost directly proportional to the number of orbits, and only three full orbits were considered here. However, the percentage gain of the SRP+PRP case over the SRP-only case does not change with the number of orbits, and it is an estimator of the gain due to PRP. In trajectories T1 and T2, the SRP can only provide a considerable amount of semi-major axis increase, due to the favourable positioning of the perigee with respect to the Sun. In particular, in trajectory T2 the SRP is mostly tangential at apogee, and therefore the increase due to PRP is small (1.84%). Conversely, the gain due to PRP is much more significant in trajectory T1 (19.89%), where the SRP only is not as effective. Instead, for trajectories T3 and T4, only the increase in semi-major axis for SRP only is negligible; this is due to the fact that in T2, the perigee arc is in the shadow, and therefore no acceleration can be provided, while in T3 the velocity points towards the Sun at perigee, and therefore the SRP is highly inefficient. For these two trajectories, the gain due to considering PRP is substantial.

From these results, it is possible to conclude that the PRP enables to perform a semi-major axis increase manoeuvre even in trajectories T3 ($\omega_0 = 180$) and T4 (270 deg), otherwise unachievable considering the SRP only. Moreover, the PRP gives an additional contribution in every study-case considered in this work.

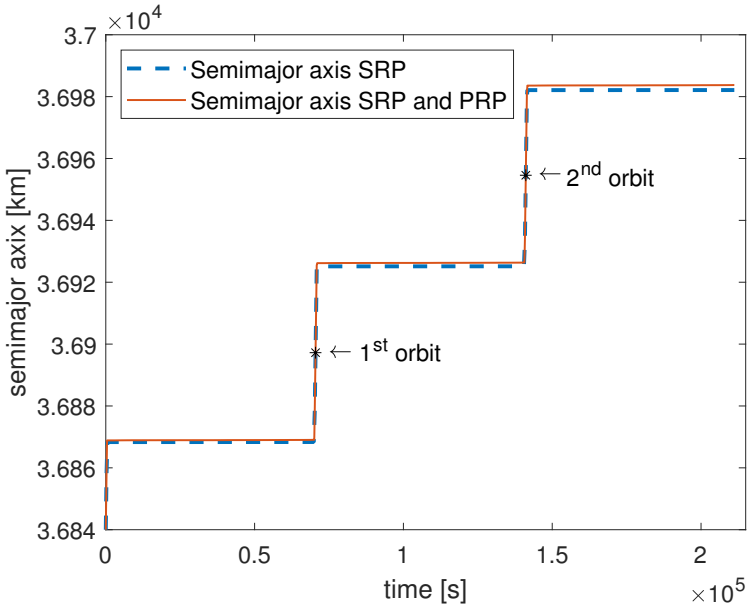

Figure 9: Semi-major axis with SRP and SRP+PRP for a sail around the Earth on T2 ($\omega = 90\,\text{deg}$).

4.2. Venus

A similar analysis was conducted for a sail around Venus. In this case, because of the high luminosity of the planet, the BBRP plays an important role in the outcome. Results are summarised in Table 6, for four trajectories starting from orbits with the same parameters as for the Earth's case, and varying periapsis (Table 4).

Table 6: Semi-major axis increase considering SRP only, SRP+PRP, and gain between the former and the latter, for Venus.

Trajectory	Increase with SRP+PRP	Increase with SRP	Gain due to PRP
T1	1.8493%	0.1861%	893.72%
T2	1.3868%	0.4738%	192.69%
T3	1.2296%	$6.8 \cdot 10^{-4}$%	180723.53%
T4	1.0780%	$2.13 \cdot 10^{-4}$%	506003.28%

As before, we analyse T2 and T3 in more detail. Fig. 14 shows trajectory T2 (starting from $\omega_0 = 90\,\text{deg}$) and the attitude of the sail. In this case the position of the arc benefits from the positive contribution of the SRP, however the dom-

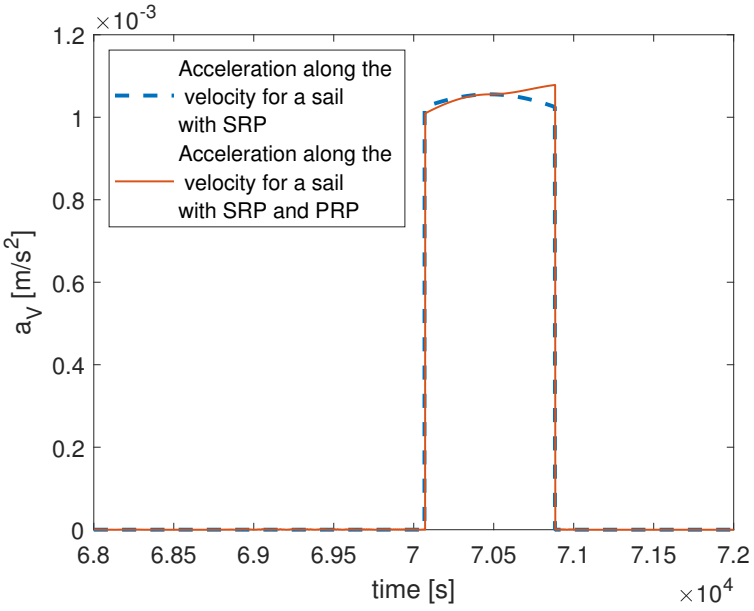

Figure 10: Tangential acceleration around the periapsis for a sail with SRP and SRP+PRP for a sail around the Earth on T2 ($\omega_0 = 90\,\text{deg}$).

inating contribution is still the planetary radiation. As regards the acceleration along the velocity direction, Fig. 16 shows the trend of the acceleration around the periapsis. A different behaviour can be highlighted at the beginning and at the end of the thrusting arc for the two cases. Considering SRP only, the sail experiences a non-null acceleration in the first part of the arc and a null one at the end to avoid negative acceleration. Instead, in the case SRP+PRP, during the first part of the arc the dominating contribution of the planet is negative, hence the sail is oriented to experience no acceleration, while in the last part the acceleration is non-null thanks to the positive contribution of the PRP. Here the presence of the PRP leads to accelerations that are 4 times larger than in the SRP-only case. Consequently, the semi-major axis increases 182.5% more in the SRP+PRP case than in the SRP-only case (Fig. 15).

We now consider trajectory T3, $\omega_0 = 180\,\text{deg}$. In this case the sail orbits along the trajectory showed in Fig. 17. As can be seen in Fig. 18, a stays almost constant when only the SRP is considered since the arc is in eclipse region and the acceleration is null in every point of the trajectory (Fig. 19). Adding the PRP enables the increase of the semi-major axis and leads to a non-zero acceleration in the pericentre arc, as can be seen in Fig. 19.

Summarising the results for Venus, the contribution of the PRP is huge, with a percentage increase over 100% for every value of ω. T1 refers to an initial orbit with the argument of the periapsis $\omega_0 = 0\,\text{deg}$. In the case of T1, the dominating contribution is always the PRP. Because of this, the sail experiences

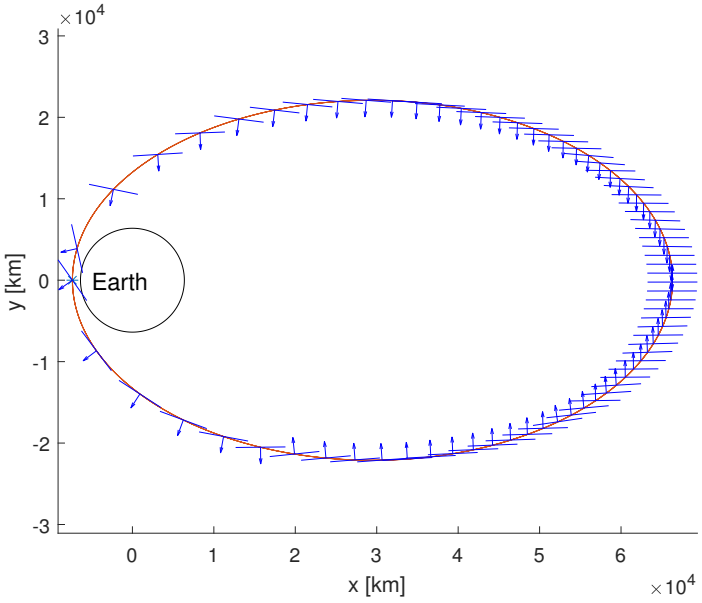

Figure 11: Trajectory around the Earth with orientation of the sail on T3 ($\omega_0 = 180\,\text{deg}$) considering SRP+PRP.

an acceleration during the thrusting arc that is up to seven times greater than the one experienced in the case SRP only. This leads to a gain in a equal to the 889.8% with respect to the SRP-only case. In the case of T4, the position of the arc is subject to the negative contribution of the Sun. For this reason, the SRP-only case leads to an almost null increment of the semi-major axis. Different results can be obtained considering the PRP, the radiation coming from the planet enables to increase a considerably. These results suggest that the consideration of the PRP for a sail orbiting around Venus is fundamental, since it enables the sail to achieve manoeuvres that would be almost unfeasible with SRP only.

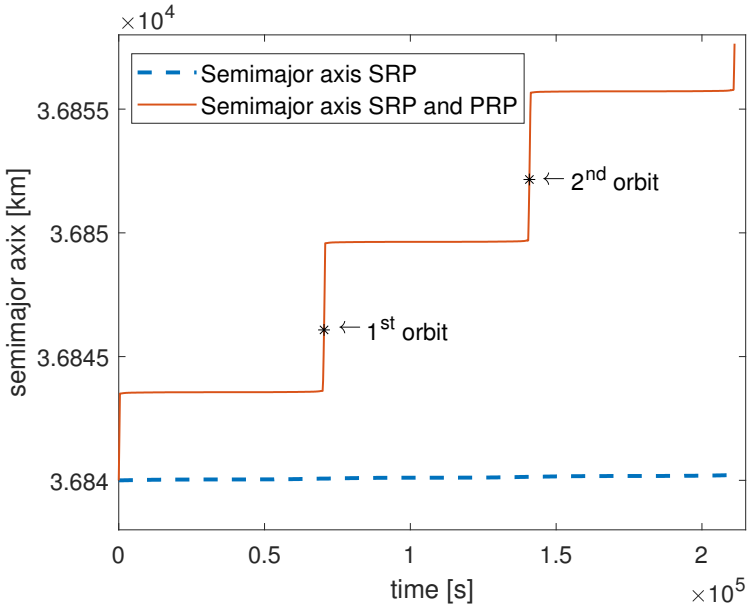

Figure 12: Semi-major axis increase with SRP and SRP+PRP for a sail around the Earth on T3 ($\omega_0 = 180\,\text{deg}$).

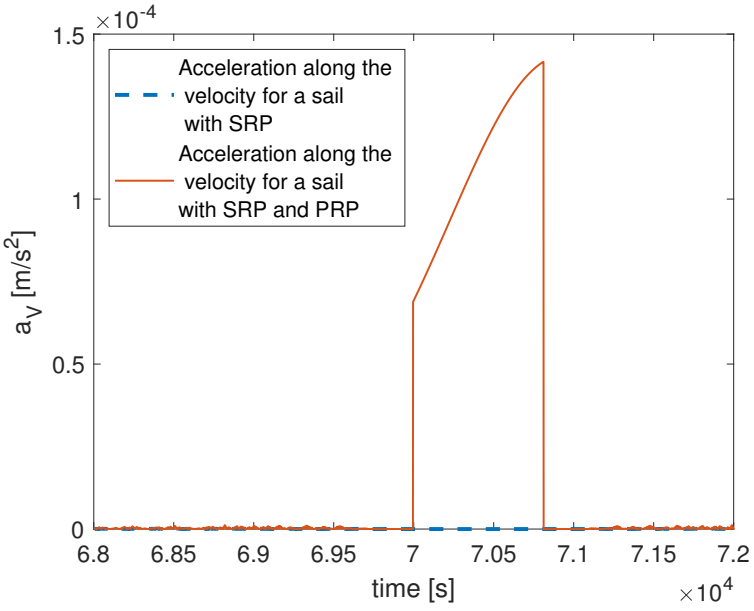

Figure 13: Tangential acceleration around the periapsis for a sail subject to SRP and SRP+PRP around the Earth on T3 ($\omega_0 = 180\,\text{deg}$).

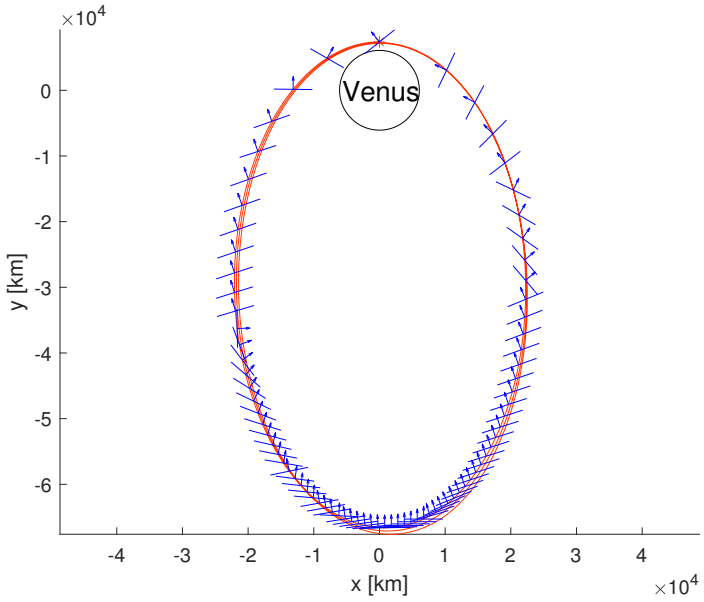

Figure 14: Trajectory around Venus with orientation of the sail on T2 ($\omega_0 = 90\,\text{deg}$)considering SRP+PRP.

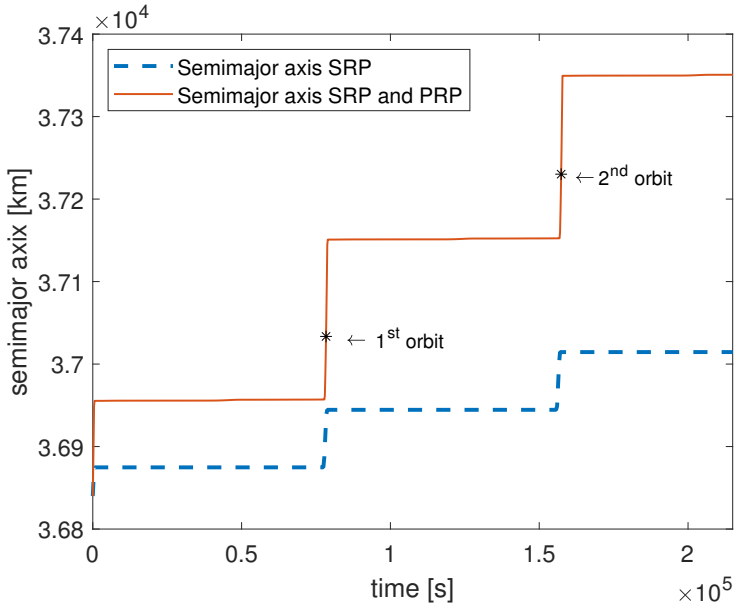

Figure 15: Semi-major axis with SRP and SRP+PRP for a sail around Venus on T2 ($\omega_0 = 90\,\text{deg}$).

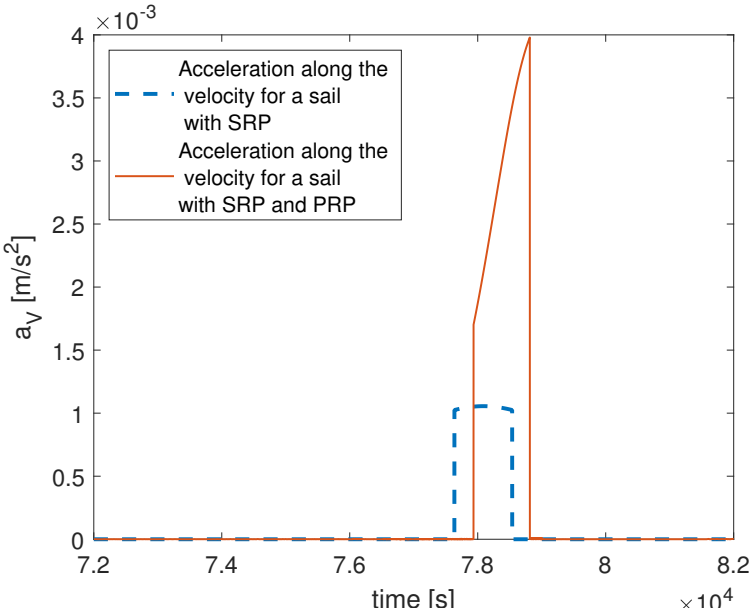

Figure 16: Tangential acceleration for a sail subject to SRP and SRP+PRP around Venus on T2 ($\omega_0 = 90\,\text{deg}$).

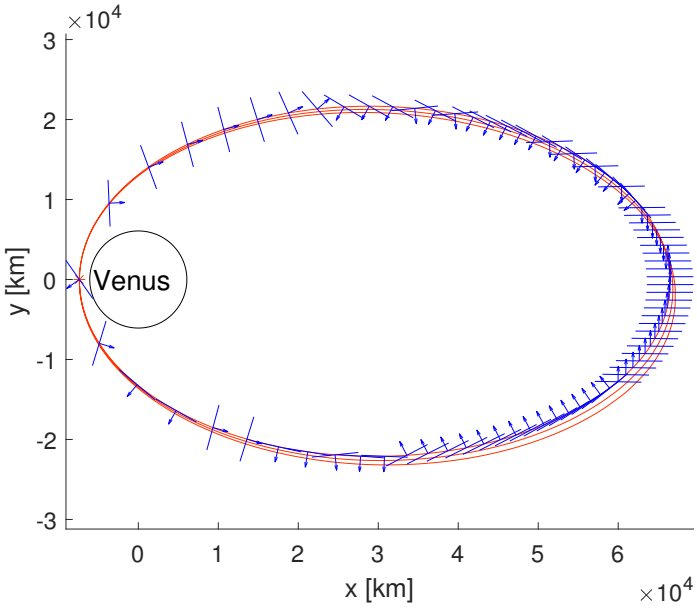

Figure 17: Trajectory around Venus with orientation of the sail on T3 ($\omega_0 = 180\,\text{deg}$) considering SRP+PRP.

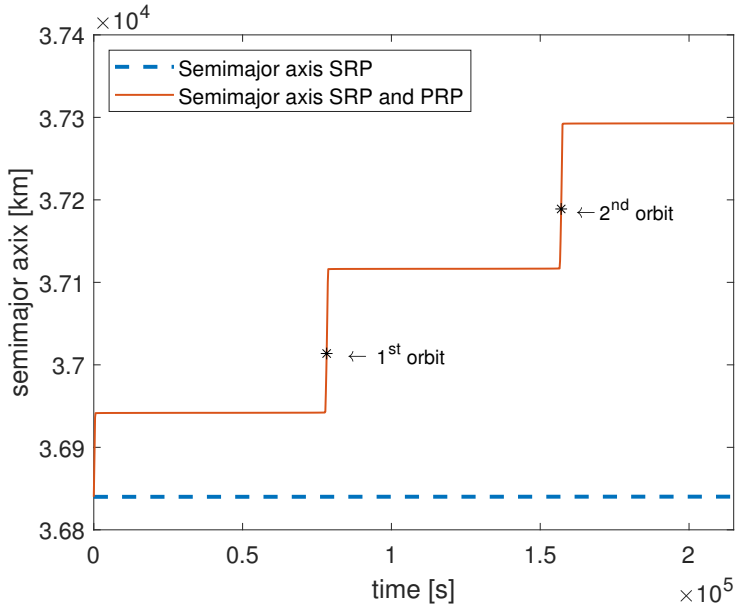

Figure 18: Semi-major axis with SRP and SRP+PRP for a sail around Venus on T3 ($\omega_0 = 180\,\text{deg}$).

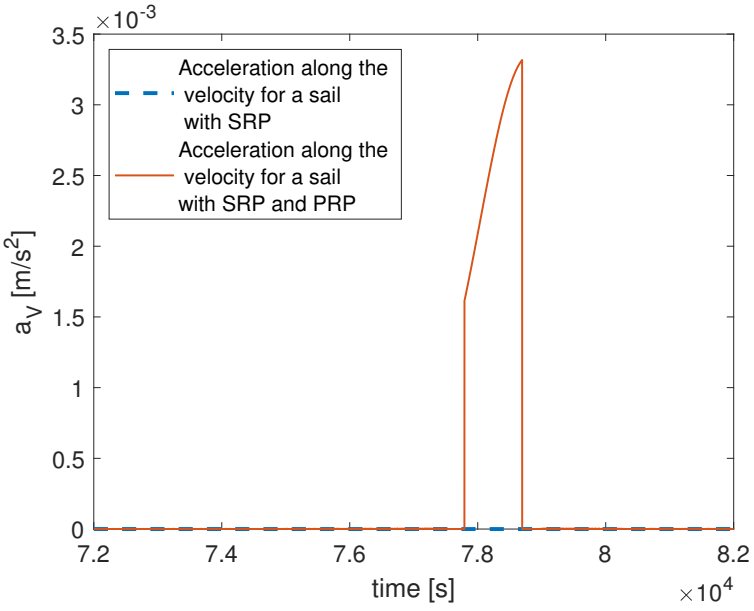

Figure 19: Tangential acceleration for a sail subject to SRP and SRP+PRP around Venus on T3 ($\omega_0 = 180\,\text{deg}$).

5. Conclusions

In this work, a solar sail orbiting around a planet has been considered, investigating the contribution of the planetary radiation pressure to the acceleration of the sail. The effects of the solar and planetary radiation pressure have been developed using opportune models that considered the optical characteristics of the sail, the directions of the incident radiations, and, in the case of the planetary radiation, the presence of black-body radiation and albedo. This has allowed the description of all possible orientations of the sail in a grid of points around the planet to maximise the acceleration along a given direction. Results in this case have shown that if the sail is orbiting around the Earth, there is not a substantial difference with the case with solar radiation only. If the considered planet is Venus, results change, with the radiation coming from the planet that becomes the dominating factor in the orientation of the sail.

Using Gauss' equations, an increasing semi-major axis manoeuvre has been integrated, using a tangential control law around Earth and Venus. Planetary radiation has a contribution in the acceleration experienced by the sail. However, in the case of a sail orbiting around the Earth this contribution is not much great, but still it can be considered as an additional factor to the force and it enables to perform a semi-major axis increase also when $\omega_0 = 180$ or 270 deg.

When a sail orbiting around Venus is considered, planetary radiation pressure is by far the dominating contribution, providing better performance of the sail, not only in the eclipse region, but everywhere close to the planet. The increase of the semi-major axis are over 100% for each position of the argument of periapsis, showing that not considering this contribution leads to worse performance of the planetary sail.

This was a preliminary study to investigate whether and how the inclusion of the radiation of the planet changes the behaviour of a sail. More accurate results could be obtained improving the models used for the planetary radiation pressure force, for the albedo, and for the eclipse. In this case, the planet was considered as a uniformly bright disc. Due to the vicinity of the sail to the planet, the consideration of the celestial body as a uniformly bright sphere emitting radial radiation could give results more consistent with reality. Moreover, the albedo so far has been modelled using an engineering approach, this model could be improved considering the portion of the planetary sphere illuminated by the Sun and the amount of the reflected light that impact the surface of the planet. As regards the eclipse region, the cylindrical eclipse model could be replaced with one considering the divergence of the Sun light rays. Moreover, since the energy coming from the planet is in the infra-red range, a study regards the material of the sail should be conducted, to analyse how the sail reflects radiation in this energy range.

To simplify the problem, a two dimensional study-case have been considered. However, the application of a three dimensional model could lead to results that consider also the out of plane variations and the assumption of a fixed Sun could be relaxed, showing a real scenario.

The results obtained in this study could be used for future works. When

a mission in the vicinity of Venus is considered, the presence of the planetary radiation should be taken into account, as the performance of the sail has dramatically improved. Moreover, for both around Venus and Earth the presence of the planetary radiation is important in the eclipse region.

Future studies can consider the combined effect of solar and planetary radiation pressure together with the effect of the aerodynamic forces. If a sail orbiting in the atmosphere of the planet is taken into account, interesting results can be obtained. In this scenario the sail is closer to the planet, experiencing also a greater planetary radiation. Further analysis could also be conducted on the optimisation of the control law, studying how it changes whether the PRP is considered or not.

Acknowledgements

Alessia De Iuliis would like to thank the James Watt School of Engineering, University of Glasgow, for hosting her for the overseas student placement between October and February, during which this work was carried out.

The authors thank an anonymous reviewer who highlighted a numerical error that slightly impacted some of the results negatively.

References

Bass, M., DeCusatis, C., Enoch, J., Lakshminarayanan, V., Li, G., Macdonald, C., Mahajan, V., Van Stryland, E., 2009. Handbook of optics, Volume II: Design, fabrication and testing, sources and detectors, radiometry and photometry. McGraw-Hill, Inc., New York.

Battin, R. H., 1999. An Introduction to the Mathematics and Methods of Astrodynamics, revised edition. American Institute of Aeronautics and Astronautics, New York.

Colasurdo, G., Casalino, L., 2001. Optimal control law for interplanetary trajectories with solar sail. Advances in the Astronautical Sciences 109(3), 2357–2368.

Coverstone, V. L., Prussing, J. E., 2003. Technique for escape from geosynchronous transfer orbit using a solar sail. Journal of Guidance, Control, and Dynamics 26 (4), 628–634.

Eguchi, S., Ishii, N., Matsuo, H., 1993. Guidance strategies for solar sail to the moon. Advances in Astronautical Sciences 85 (2), 1419–1433.

Fekete, T. A., 1992. Trajectory design for solar sailing from low-earth orbit to the moon. Ph.D. thesis, Massachusetts Institute of Technology.

Frisbee, R., Brophy, J., 1997. Inflatable solar sails for low-cost robotic mars missions. In: 33rd Joint Propulsion Conference and Exhibit. p. 2762.

Gao, Y., 2007. Near-optimal very low-thrust earth-orbit transfers and guidance schemes. Journal of guidance, control, and dynamics 30 (2), 529–539.

Garner, C., Prince, H., Edwards, D., Baggett, R., July 2001. Developments and activities in solar sail propulsion. In: 37th Joint Propulsion Conference and Exhibit. Salt Lake City, UT, USA, pp. 3234.

Grøtte, M. E., Holzinger, M. J., 2017. Solar sail equilibria with albedo radiation pressure in the circular restricted three-body problem. Advances in Space Research 59 (4), 1112–1127.

Lappas, V., Mengali, G., Quarta, A., Gil-Fernandez, J., Schmidt, T., Wie, B., 2009. Practical systems design for an earth-magnetotail-monitoring solar sail mission. Journal of Spacecraft and Rockets 46 (2), 381–393.

Larson, W., Wertz, J. R., 1992. Space mission analysis and design. Tech. rep., Torrance, CA (United States); Microcosm, Inc.

Leipold, M., 2000. Solar sail mission design. Ph.D. thesis, Deutsches Zentrum für Luft-und Raumfahrt.

Leipold, M., Seboldt, W., Lingner, S., Borg, E., Herrmann, A., Pabsch, A., Wagner, O., Brückner, J., 1996. Mercury sun-synchronous polar orbiter with a solar sail. Acta Astronautica 39 (1-4), 143–151.

Lyle, R., Leach, J., Shubin, L., 1971. Earth albedo and emitted radiation. NASA SP-8067.

Macdonald, M., Hughes, G., McInnes, C., A. Lyngvi, P. F., Atzei, A., 2007. Geosail: an elegant solar sail demonstration mission. Journal of Spacecraft and Rockets 44 (4), 784–796.

Macdonald, M., McInnes, C., 2005. Realistic earth escape strategies for solar sailing. Journal of Guidance, Control, and Dynamics 28 (2), 315–323.

Macdonald, M., McInnes, C., 2011. Solar sail science mission applications and advancement. Advances in Space Research 48 (11), 1702–1716.

McInnes, C., 1999. Solar Sailing. Technology, Dynamics and Mission Applications. Springer-Praxis Books in Astronautical Engineering. Springer-Verlag, Berlin.

Mengali, G., Quarta, A. A., 2005. Near-optimal solar-sail orbit-raising from low earth orbit. Journal of Spacecraft and Rockets 42 (5), 954–958.

Mengali, G., Quarta, A. A., Lappas, V. J., 2007. Optimal steering law for the geosail mission. Journal of guidance, control, and dynamics 30 (3), 876–879.

Schaub, H., Junkins, J. L., 2018. Analytical Mechanics of Space Systems. American Institute of Aeronautics and Astronautics, 1801 Alexandre Bell Drive, Reston, Virginia.

Stefan, J., 1879. Über die beziehung zwischen der wärmesthaltung und der temperatur (regarding the relationship between heat radiation and temperature). Sitzungsberichte der Mathematisch-naturwissenschaftlichen Classe der Kaiserlichen Akademie der Wissenschaften 79, 391–428.

Stolbunov, V., Ceriotti, M., Colombo, C., McInnes, C., 2013. Optimal law for inclination change in an atmosphere through solar sailing. Journal of Guidance, Control, and Dynamics 36 (5), 1310–1323.

Thornton, E. A., 1996. Thermal structures for aerospace applications. American Institute of Aeronautics and Astronautics, 1801 Alexandre Bell Drive, Reston, Virginia.